Journal of Applied Polymer Science

Scalable production of polymer nanofiber-based ropes, cables, and coatings

Christopher R. Frank, Johnson Samuel
Department of Mechanical Aerospace and Nuclear Engineering, Rensselaer Polytechnic Institute, 110 8th Street, Troy, New York 12180
Correspondence to: J. Samuel (E-mail: samuej2@rpi.edu)

ABSTRACT: This article presents a single, scalable manufacturing process for the continuous production of nanofiber-based ropes, cables, microscale wire coatings, and multimaterial mats. The ropes, cables, and wire coatings were manufactured with a cascading electrospinning setup that was used in conjunction with a rotating ring collector and a take-up reel. The fibrous mats were realized by replacing the ring collector with a directed nozzle. Both configurations allowed for nanofiber architectures with multiple layers and material combinations. The tensile failure patterns of the cables revealed distinct effects of the multimaterial sheaths. The adhesion strength and load–displacement profiles for the nanofiber coating interfaces were observed to be polymer-specific. For multimaterial mats, the cospinning of the polymers resulted in a blended mechanical behavior for the composite mats, in contrast to the sequential ply failure observed in laminated mats. © 2016 Wiley Periodicals, Inc. J. Appl. Polym. Sci. **2016**, *133*, 43747.

KEYWORDS: electrospinning; fibers; manufacturing

Received 27 November 2015; accepted 5 April 2016
DOI: 10.1002/app.43747

INTRODUCTION

Recent innovations in the areas of smart textiles,[1] biomedical manufacturing,[2] soft actuators,[3] and three-dimensional (3D) printing of fiber-reinforced soft composites[4] have highlighted the need to develop manufacturing processes for multimaterial polymer nanofiber yarns and fibrous coatings. Figure 1(a-c) outlines some of the key nanofiber architectures of interest in these applications. Nanofiber-based ropes [Figure 1(a)], as the name suggests, are comprised of a series of nanofibers that are twisted in the form of a rope.[5] Although the diameter of the individual nanofibers themselves could be in the 10–500 nm range, the diameter of the rope could vary in the 10–500 μm range. Figure 1(b) outlines the structure of multimaterial cables that have a nanofiber rope at its central core. This core is, in turn, surrounded by multiple sheaths [two highlighted in Figure 1(b)] of different polymer nanofibers. The cable architecture can also be extended to create nanofiber coatings on microscale wires, as shown in Figure 1(c). In addition to these specialized architectures, fibrous mats are a more commonly used form of nanofibers.[6] The realization of a single scalable manufacturing pathway for all of these nanofiber architectures has the potential to deliver innovative solutions for applications in the biomedical, aerospace, and defense sectors.[7]

The electrospinning process is common to the four fiber architectures of interest, namely, nanofiber-based ropes, cables, microscale wire coatings, and multimaterial mats.[8–13] The manufacturing of nanofiber ropes is a two-stage process that first involves the manufacturing of polymer nanofibers using electrospinning, followed by a subsequent twisting operation to manufacture the rope. This process was recently demonstrated by Baniasadi *et al.*[5] to manufacture poly(vinylidene fluoride) (PVDF) nanofiber ropes. However, their manual twisting operation made the process infeasible for scalable production. Ali *et al.*[14] overcame this shortcoming by using a rotating, cone-shaped metallic collector, in conjunction with a motorized take-up reel, to form the ropes. Although this manufacturing technique was effective for the scalable production of ropes, it cannot be used for the other architectures of interest.

The coating of microscale wires (50–500 μm diameter) with polymer nanofibers has applications for smart textiles and soft actuators.[1,3] The challenge involved here is that of ensuring a conformal fiber coating without breaking the microwire. Currently, there appears to be a dearth of manufacturing processes that can achieve this. The directed deposition of multimaterial fiber mats is particularly relevant to the nascent field of the 3D printing of fiber-reinforced soft composites.[4] The electrospinning-based fiber mat manufacturing techniques used for this 3D printing operation are currently not capable of providing on-the-fly material switching capabilities while laying down the fibrous structures.[4]

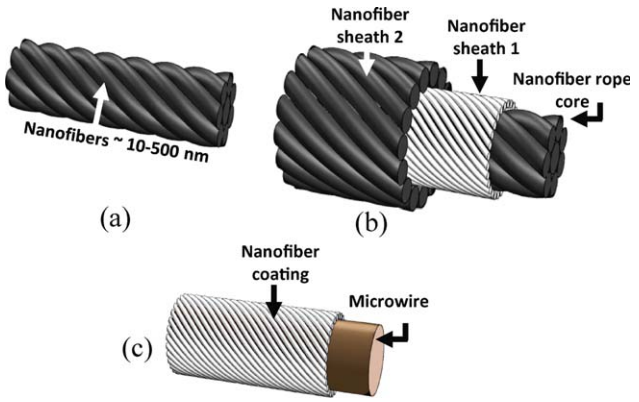

Figure 1. Key nanofiber architectures of interest: (a) ropes, (b) sheathed multimaterial cables, and (c) fibrous coating on microscale wires. [Color figure can be viewed in the online issue, which is available at wileyonlinelibrary.com.]

In light of the aforementioned manufacturing needs, the objective of this research was to develop a single, scalable manufacturing process that allowed for the continuous production of nanofiber-based ropes, cables, microscale wire coatings, and multimaterial mats. The ropes, cables, and wire coatings were achieved with a novel cascading electrospinning setup, in conjunction with a rotating ring collector and a take-up reel. The multimaterial fibrous mats were realized by replacing the ring collector with a directed nozzle. To our knowledge, this is the first report of the use of a single scalable manufacturing process that allows for the continuous production of the different nanofiber architectures. The nanofiber-based cables and the microscale wire coatings are also the first of their kind to be reported in the literature. In addition to the manufacturing process, we also present material characterization data related to the various fiber architectures.

The remainder of this article is organized as follows. First, the Experimental section presents the overall manufacturing process flow for each of the different fiber architectures. This is followed by the results of the characterization of the fiber architectures. Finally, the specific conclusions that can be drawn from this work are presented.

EXPERIMENTAL

Novel Scalable Manufacturing Process

This section presents the manufacturing process used for the continuous production of nanofiber-based, ropes, cables, microscale wire coatings, and multimaterial mats. The creation of these fiber architectures primarily relies on the use of the far-field solution electrospinning process.[5,6] In the following subsections, we first describe the setup used for manufacturing single-material nanofiber ropes. This is followed by the setups for manufacturing multimaterial cables and nanofiber coatings on microscale wires, both of which build on the technique used for the ropes. Finally, the use of a directed nozzle to create multimaterial mats is presented.

Nanofiber Ropes

Figure 2(a) outlines the manufacturing setup used to create the nanofiber ropes. As seen, the setup consisted of two electrospinning syringe pumps facing an aluminum ring collector. The ring collector rode on four bearings and was rotated with a belt drive connected to a 50-W brushed direct-current motor equipped with a controller. For the experiments conducted in this study, the diameter of the ring collector was kept constant at 7.62 cm. However, this diameter could be changed to influence the twist of the rope for specific polymer applications. During the manufacturing process, the two-syringe pumps were charged with opposite-polarity, high voltage, whereas the ring collector was maintained as the ground electrode.

Figure 2(b) depicts the sequence of operations used to manufacture the nanofiber ropes.

In step 1, the two-syringe pumps with opposite electrical polarities were placed facing each other. The electrospinning process was started on both syringes by making the nanofibers spin toward their oppositely charged counterpart. This process resulted in the formation of suspended nanofibers that were nearly equidistant from both syringe pumps.

In step 2, this fibrous mass was directed with a 0.56 m/s air current produced by a duct fan to enable the attachment of the fibers to the rotating ring collector until the fibers formed a continuous mesh across the opening of the ring collector.

In step 3, to initiate the spooling of the rope, a glass rod was manually placed in the path of the nanofibers being directed to

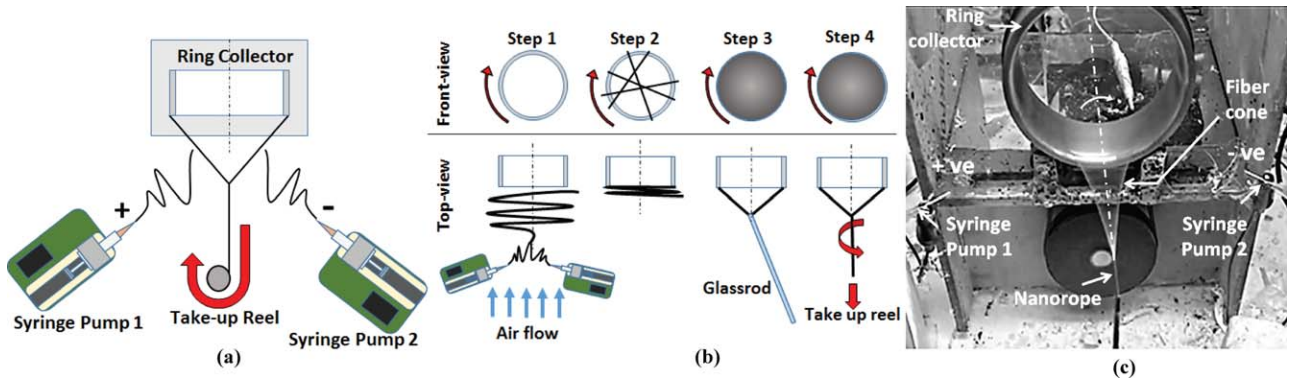

Figure 2. Nanofiber-based rope manufacturing: (a) overall configuration, (b) sequence of operations, and (c) production demonstration. [Color figure can be viewed in the online issue, which is available at wileyonlinelibrary.com.]

the ring collector. This enabled the fibers to attach to both the glass rod and the ring collector.

In step 4, the glass rod (with the fibers attached) was then drawn manually toward the take-up reel. At this stage, the rotation of the ring collector imparted a twist to the nanofibers, and this resulted in the creation of the ropes. Once the process was initiated, the take-up reel continued to wind the rope onto its spool.

Figure 2(c) depicts the production of the nanofiber ropes using the aforementioned setup. It should be noted here that unless the electrospinning process was stopped at any instant, the rotation of the take-up reel resulted in a continuous production of the ropes. The angle of twist in the rope could be controlled by changing the relative difference between the rotational velocity of the ring collector and the linear velocity imparted to the rope by the take-up reel.

In this study, two candidate polymers were chosen for manufacturing the nanofiber ropes, namely, PVDF and nylon-6. PVDF was chosen because of its piezoelectric nature.[5] Nylon 6 was chosen because it is a proven electrical insulator and also has applications in the biomedical and fiber-reinforced soft composite domain.[15] Nylon 6 pellets (3 mm in diameter), formic acid (reagent grade > 95%), dimethylformamide (anhydrous, 99.8%), acetone (> 99.9%), PVDF pellets (3 mm in diameter), and tetrabutyl ammonium chloride (> 97%) were all obtained from Sigma-Aldrich and were used as received. To manufacture the nylon ropes, a solution of 17.5 wt % nylon 6 in formic acid was prepared and used along with a 21-gauge steel needle. For the PVDF ropes, a solution of 17.5 wt % PVDF and 3 wt % tetrabutyl ammonium chloride in 50:50 dimethylformamide/acetone was prepared and used with a 25-gauge steel needle. The nylon and PVDF solutions were delivered with Razel R99EJM syringe pumps operating at flow rates of 1.15 and 1.65 mL/h, respectively. Because of the difference in the viscosities of the two solutions, the values for their specific flow rates and needle sizes were chosen to ensure a constant flow of the solution without starving the needle tip. The syringe pumps were placed such that the needle tips were 15 cm apart. The ring collector was rotated at 500 rpm, whereas the linear collection speed of the rope was set to 200 mm/min. The collection speed of the rope was controlled via the use of a 24 V gear motor run at 3 V.

Figure 3(a–c) depicts the images of the nylon and PVDF ropes created from this process. The diameters of the ropes were 100 and 185 μm, respectively [Figure 3(b,c)], with overall lengths in the 1–2 m range. The nylon and PVDF nanofibers themselves had diameters of 60 and 500 nm, respectively, as shown in the inset of Figure 3(b,c). The primary angles of twist of the nylon and PVDF ropes were 30 and 36°, respectively. These values were measured digitally from the scanning electron microscopy images through the calculation of the angle between the lay direction of the fibers and the axis of the rope. In addition to the primary twist generated by the rotating ring collector, the PVDF ropes were also able to withstand an overtwisting operation that resulted in the formation of PVDF coils (~63° twist), as shown in Figure 3(d). Because of their low strain to failure, the nylon ropes could not withstand the overtwisting operation to form the coils.

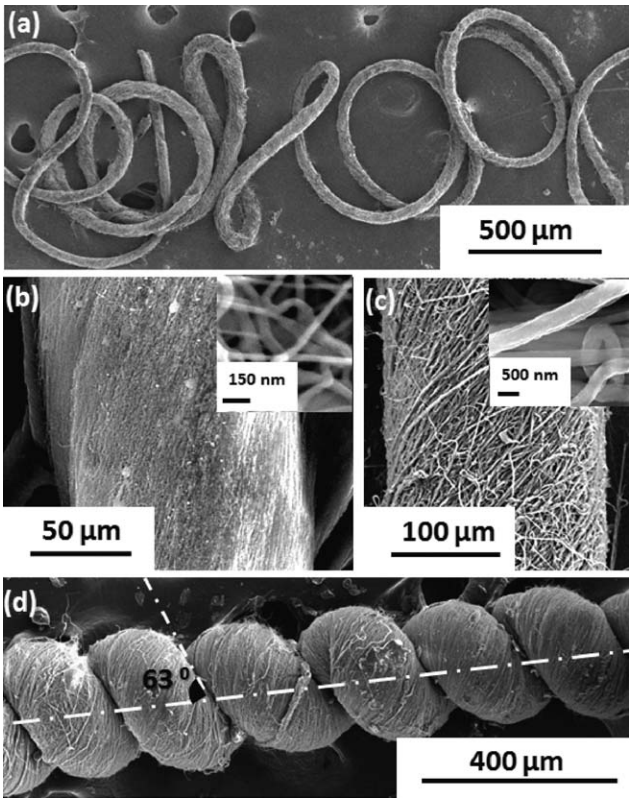

Figure 3. Scanning electron microscopy images of nanofiber ropes: (a) overall structure, (b) nylon 6 rope, (c) PVDF rope, and (d) PVDF coil with a secondary twist.

Nanofiber Cables

The manufacturing process for nanofiber cables is outlined in Figure 4(a) for a cable composed of a nanofiber rope (core) encased in a single polymer sheath. As shown in Figure 4(a), the setup consisted of a cascading system of electrospinning units similar to that used for the manufacturing of the nanofiber ropes [Figure 2(a)]. The primary fiber production unit [the first electrospinning unit in Figure 4(a)] was responsible for manufacturing the rope at the core of the cable. This rope was then passed through the center of a secondary rotating ring collector and its associated electrospinning setup [Figure 4(a)]. The syringe pumps dedicated to the deposition of nanofibers to this secondary ring collector were responsible for the formation of the polymer sheath around the rope at the core. The resulting nanocable was then continuously wound onto the take-up reel.

The specific processing steps involved in manufacturing a cable composed of a nanofiber rope (core) encased in a single polymer sheath were as follows [Figure 4(b)].

In step 1, the core nanofiber rope was first created with the steps outlined in Figure 2(b).

In step 2, this core nanofiber rope was then fed through the secondary ring collector in the direction of the spooling of the cable [denoted by arrows in Figure 4(b)]. The voltage sources and syringe pumps were then turned on to start the electrospinning process to deposit the sheath layer of nanofibers.

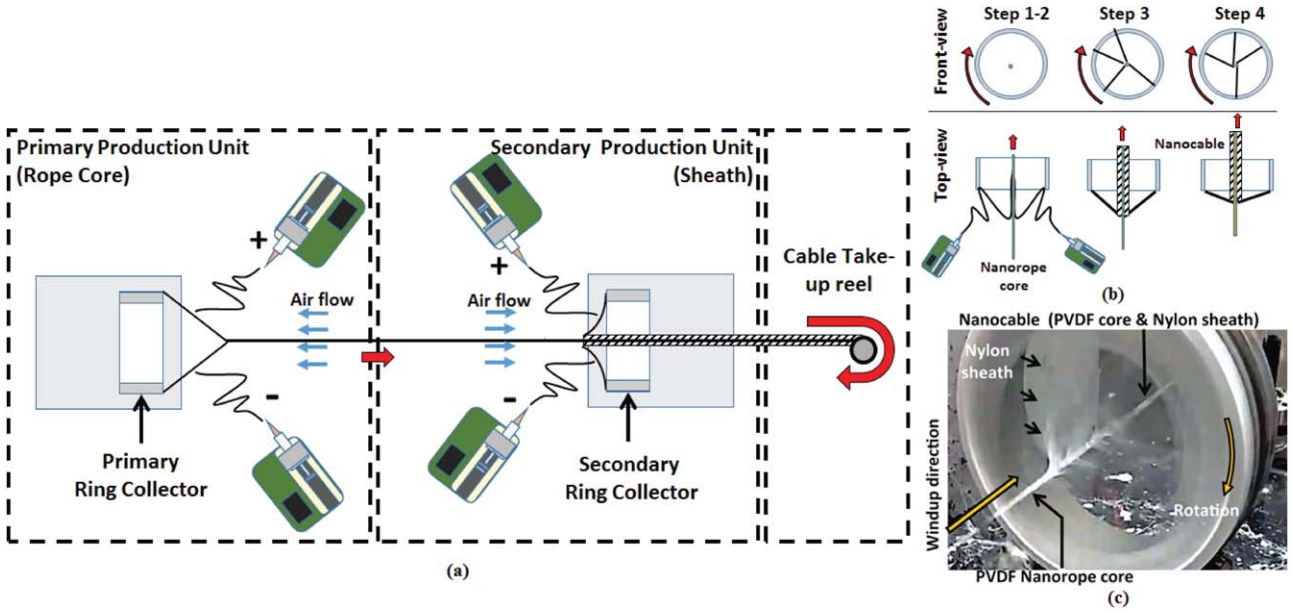

Figure 4. Cable manufacturing (core and a single sheath): (a) overall configuration, (b) sequence of operations, and (c) production demonstration. [Color figure can be viewed in the online issue, which is available at wileyonlinelibrary.com.]

In step 3, as the rope was fed through, the sheath polymer established a fibrous cone between the rope and the secondary ring collector.

In step 4, the rotation of the secondary ring collector relative to the rope core wound the polymer sheath around the core.

The implementation of this cable manufacturing process is shown in Figure 4(c), where the core PVDF rope was passed through the secondary ring collector that spins a nylon sheath around the PVDF rope. At each of the cascading units, the electrospinning conditions (i.e., voltage, electrode gap, flow rate, needle diameters, and airflow rate) were maintained at the polymer-specific values reported under the subsection on nanofiber ropes. The uniqueness of the process lies in the fact that the hollow ring-shaped collector allows for the use of a cascading system of downstream electrospinning units to manufacture cables with multiple sheaths. Figure 5 depicts the cross section of such a multisheath cable. As shown, the cable had a PVDF rope at the core that was encased by an intermediate nylon nanofiber sheath; this, in turn, was encased in an outer PVDF nanofiber sheath. This multisheath cable was produced with three cascading electrospinning units with the primary one spinning PVDF to make the rope core [Figure 4(a)]. Nylon and PVDF were then spun separately at each of two downstream units to yield the cable architecture depicted in Figure 5. The overall length of these multisheath cables was comparable to that seen for the ropes in Figure 3(a).

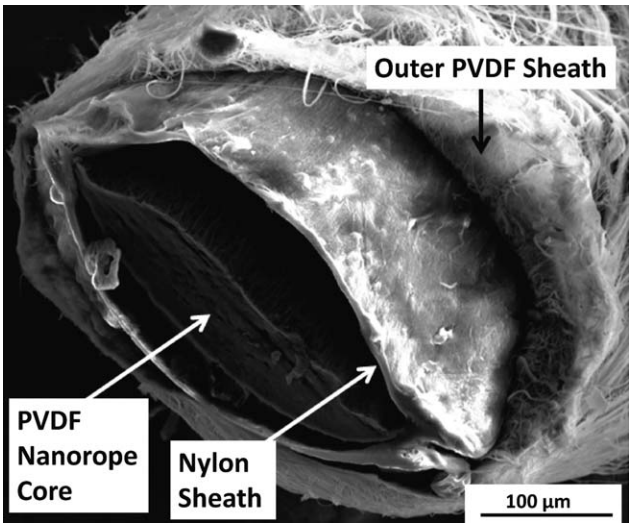

Figure 5. Cut cross-section of a multisheath cable.

Nanofiber Coatings on Microscale Wires

The process developed for manufacturing the cables [Figure 4(a)] was extended to achieve conformal coating of microscale wires with polymer nanofibers. This was achieved by replacing the primary fiber production unit (responsible for the rope at the core of the cable), with a spool that fed the microscale wire into the secondary ring collector setup [Figure 4(a)].

For this study, we coated two copper wires of 75 and 500 µm diameter by feeding them through the secondary ring collector (500 rpm) at a take-up speed of 200 mm/min. This range of wire diameters was specifically chosen because of its relevance for biomedical applications, such as surgical wires and aneurysm coils.[15,16] Wires with diameters smaller than 75 µm were observed to break during handling and, as such, could not be tested. During this coating process, the wire was observed to undergo a slight deflection [θ in Figure 6(a)] when acted upon by the electrospun fibers. This deflection angle was estimated to be about 8–10° using trigonometric ratios involving the distance of the spool from the ring collector and the horizontal deflection of the wire. Both these distances were calculated from an in-process digital image.

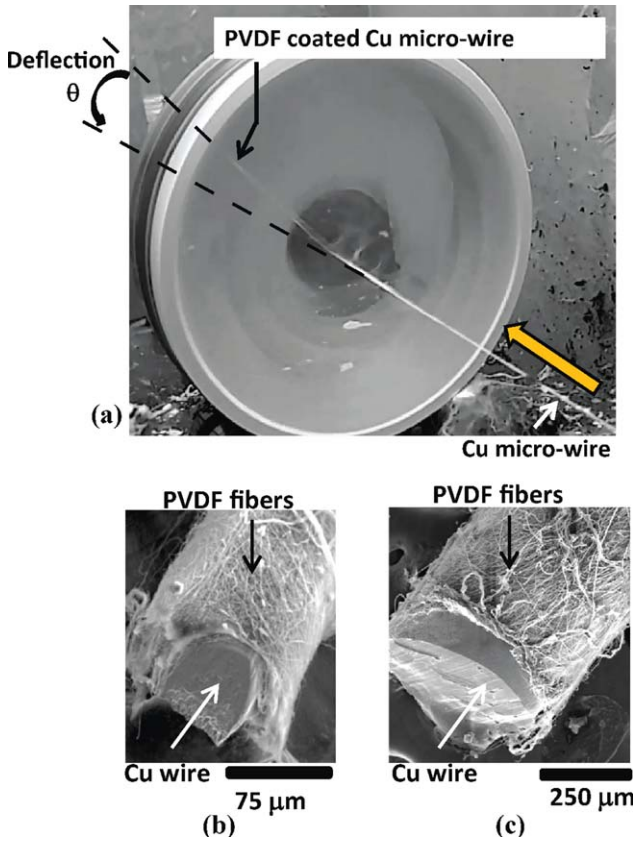

Figure 6. PVDF fiber coatings on microscale wires: (a) production demonstration, (b) coating on a 75-μm wire, and (c) coating on a 500-μm wire. [Color figure can be viewed in the online issue, which is available at wileyonlinelibrary.com.]

The deflection issue was not critical for manufacturing the cables (Figure 5) because the low stiffness of the core nanofiber rope accommodated for this deflection. However, in the case of metal microscale wires, the stiffness of the wire varied as a function of the diameter, and this, in turn, affected the quality of the coating achieved. The low stiffness of the 75-μm copper wire was observed to readily accommodate this deflection; this resulted in a noticeable angle of twist for the coated fibers [Figure 6(b)]. On the other hand, the stiffer 500-μm copper wire was less forgiving of this deflection, the result of which was more of a random fiber coating on the wire [Figure 6(c)]. On average, the coatings obtained were about 15 μm thick.

Although copper microwires have been used as an example here, both conductive and nonconductive microwires could be coated with this process. Such coated microwire structures have applications in medical sutures and fiber-insulation.[16]

Multimaterial Nanofiber Mats

The goal of this next process modification was to enable the setup used for manufacturing nanofiber ropes to also accommodate the manufacture of multimaterial fibrous mats. This was accomplished by replacing the ring collector [Figure 2(a)] with a custom nozzle, as shown in Figure 7(a). The fibers generated by the nozzles were directed to the surface being coated using an air stream (0.56 m/s). The fact that this two-syringe configuration eliminated the need for a ground electrode made it suitable to deposit mats on the nonconducting substrates. Depending on the polymer solution loaded into the syringe pumps, one could either manufacture layered multimaterial mats or cospun mats. Figure 7(b) shows a two-layered laminated mat produced by alternating between the deposition of nylon 6 and PVDF nanofibers, whereas Figure 7(c) shows a mat where both the PVDF and the nylon 6 nanofibers were cospun to generate an intertwined fibrous structure. The mats obtained from this setup were observed to have a slight radial variation in their thickness, with a more uniform thickness being measured close to the center of the nozzle.

Beyond applications to filters and fibrous coatings, this adaptation of the electrospinning process is also well-suited for the 3D printing of fiber-reinforced soft composites.[4] This 3D printing process demonstrated by Spackman *et al.*[4] involves the layer-by-layer integration of electrospun fibers into a UV-curable polymer matrix that is dispensed from an inkjet nozzle. Because the nanofiber deposition head [Figure 7(a)] can be easily integrated onto the Spackman *et al.*[4] 3D printing platform, it is expected to allow for a relatively easy deposition of a variety of fibrous mats during the 3D printing of fiber-reinforced soft composites.

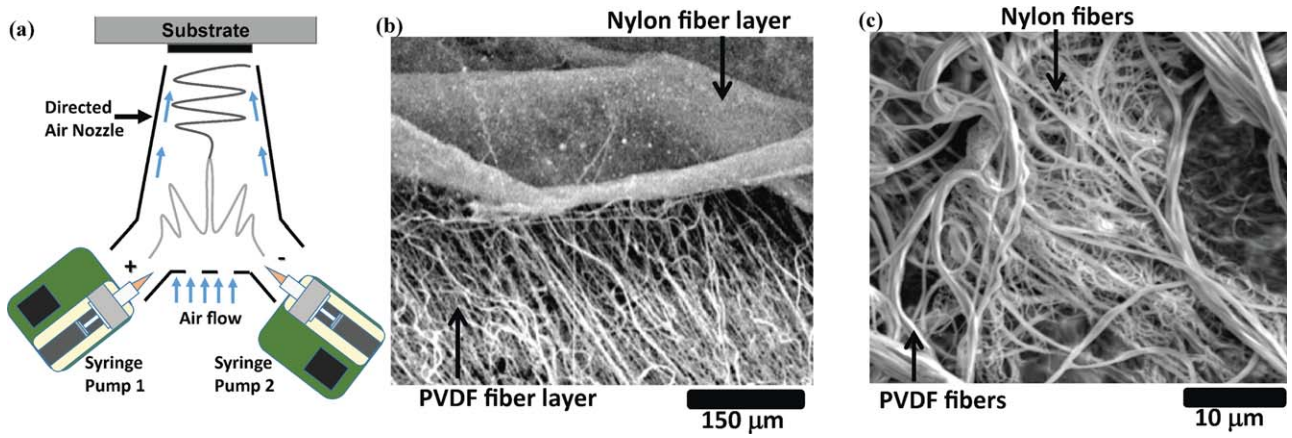

Figure 7. Large-area deposition of multimaterial fibrous mats: (a) overall configuration, (b) laminated mat (nylon plus PVDF), and (c) cospun mat (nylon plus PVDF). [Color figure can be viewed in the online issue, which is available at wileyonlinelibrary.com.]

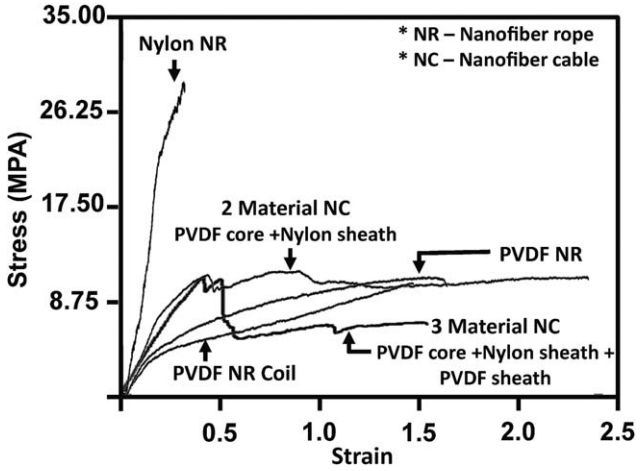

Figure 8. Tensile testing data of the nanofiber ropes and cables.

RESULTS AND DISCUSSION

Characterization of the Fiber Architectures

Tensile Testing of the Ropes and Cables. The tensile properties of the nanofiber-based ropes and cables were characterized at a strain rate of about 0.0093 s^{-1} with a custom-built testing unit.[4] Friction clamps were used in combination with a thermal glue to secure the ends of the ropes onto a Mikrotools DT-110 precision motion platform (±1 μm positional accuracy). A Kistler 9256C dynamometer was used to capture the load–displacement data. Five replicates were conducted for each of the test cases, namely, nylon rope, PVDF rope, PVDF coil, single-sheath cable (PVDF core + nylon sheath), and multisheath cable (PVDF core + nylon sheath + PVDF sheath). Figure 8 depicts the representative engineering stress–strain curves seen for these five cases. Table I summarizes the key properties from the tensile tests.

The results show that the nylon nanofiber ropes had a higher Young's modulus and a lower strain-to-failure when compared to the PVDF ropes. For any given strain value, the PVDF coils could only bear a lower stress when compared to the PVDF ropes. This is suspected to be caused by the untwisting of the coils under the applied load. The single-sheath cable composed of the PVDF core and the nylon sheath showed the combined effect of both materials. This was attributed to the method of failure seen within the single-sheath cable [Figure 9(a–c)]. As shown in Figure 9(a–c), the nylon sheath and PVDF failed at different locations along the cable. The nylon sheath was the first to fail, as shown by the drop in the stress–strain curve around a strain value of 0.5. Once the nylon sheath failed, the PVDF core had to overcome the interfacial friction of the nylon sheath before it could be fully loaded to failure. This allowed the single-sheath cable to handle a larger overall strain of 2.12 ± 0.31.

The scanning electron microscopy image of the multisheath cable showed the nylon sheath failing in line with the PVDF core and the outer sheath layer [Figure 9(d)]. This failure mode corresponded to the ultimate failure of the cable at a strain value of 1.59 (Figure 8). However, because of the sizable drop in the stress value observed at a strain of 0.5 (Figure 8), we suspect that the nylon sheath failed first at this lower strain value. Beyond this point, the load was primarily carried by the PVDF core and outer sheath, whereas the ruptured nylon sheath was held sandwiched between the two. This continued until a strain of 1.59 was reached when the PVDF core and outer sheath failed; resulting in a second in-line rupture of the nylon sheath [Figure 9(d)].

Adhesion Strength of the Microscale Wire Coatings. To measure the adhesion strength of the microscale wire coatings, a test was designed [Figure 10(a)] to generate the load–displacement curves for the coating interface under conditions of shear loading. Because of the fragility of the 75 μm wire, only the 500 μm wire was tested for the interfacial strength of the coating. The uncoated section of the wire was first passed through a 510-μm diameter hole made in an aluminum block attached to a Kistler 9256C three-axis dynamometer. The wire was then pulled co-axially with respect the drilled hole with a precision three-axis motion platform.

Figure 10(b) depicts the load–displacement curve for the 500-μm wire recorded over an overall coating length of 6 mm. The normalized displacement (ND) was used for the purposes of the plot with an ND of 1 corresponding to a 6-mm length. As indicated by the difference in the heights of the load–displacement curves, the PVDF nanofiber coating had a stronger adhesion to the microwire when compared to the nylon nanofibers. The PVDF coating exhibited a bilinear curve with the failure of the coating occurring at a displacement of 4.5 mm (ND = 0.75). The nylon coating, on the other hand,

Table I. Mechanical Properties of Nanofiber Ropes and Cables

Material	Young's modulus (MPa)	Ultimate tensile stress (MPa)	Ultimate tensile strain
Nylon nanofiber rope	109.99 ± 5.64	34.41 ± 2.48	0.37 ± 0.06
PVDF nanofiber rope	27.75 ± 7.02	16.04 ± 4.10	1.65 ± 0.42
PVDF nanofiber coil	18.82 ± 4.32	12.78 ± 1.84	1.70 ± 0.27
Single-sheath nanofiber cables (PVDF core plus nylon sheath)	41.93 ± 9.19	15.46 ± 2.57	2.12 ± 0.31
Three-material nanofiber cables (PVDF core plus nylon sheath plus PVDF sheath)	27.40 ± 2.74	9.39 ± 1.65	1.35 ± 0.19

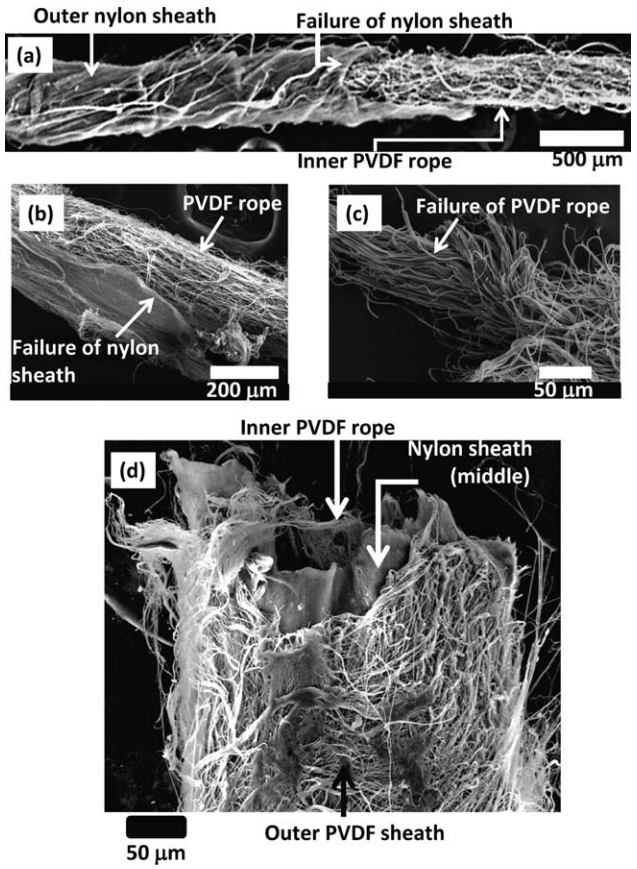

Figure 9. Cable failure mechanisms: (a) single-sheath cable, (b) close-up of a single-sheath cable failure of the sheath, (c) close-up of a single-sheath cable failure of the PVDF core, and (d) multisheath cable failure.

exhibited a trapezoidal curve. It had a linear increase until the onset of the sliding at a displacement of 3.9 mm (ND = 0.65). The load stayed more or less constant until the displacement of 5 mm (ND = 0.83), after which there was a linear decay in the load value. This difference in the shape of the load–displacement curves could be explained by the nature of the stripped coatings when observed under the scanning electron microscope. The stripped nylon sheath showed distinct folds along its exterior [arrows in Figure 10(c)], which were clearly absent in the case of the stripped PVDF sheath [Figure 10(d)]. The formation of these folds indicates a progressive failure of the interface, which could explain the constant portion of the trapezoidal load–displacement curve for nylon (between the NDs of 0.65 and 0.83). The absence of these folds in the stripped PVDF implies a near instantaneous failure of the interface at an ND of 0.75 that results in a bilinear curve.

Tensile Properties of the Multimaterial Nanofiber Mats. To characterize the tensile properties of the nanofiber mats, the fibers were first deposited continuously for 20 min with the directed nozzle [Figure 7(a)]. The mats were then cut from the region close to the center of the nozzle that exhibited a uniform thickness. In addition to the single-material nylon and PVDF mats, the laminated and cospun multimaterial mats [shown in

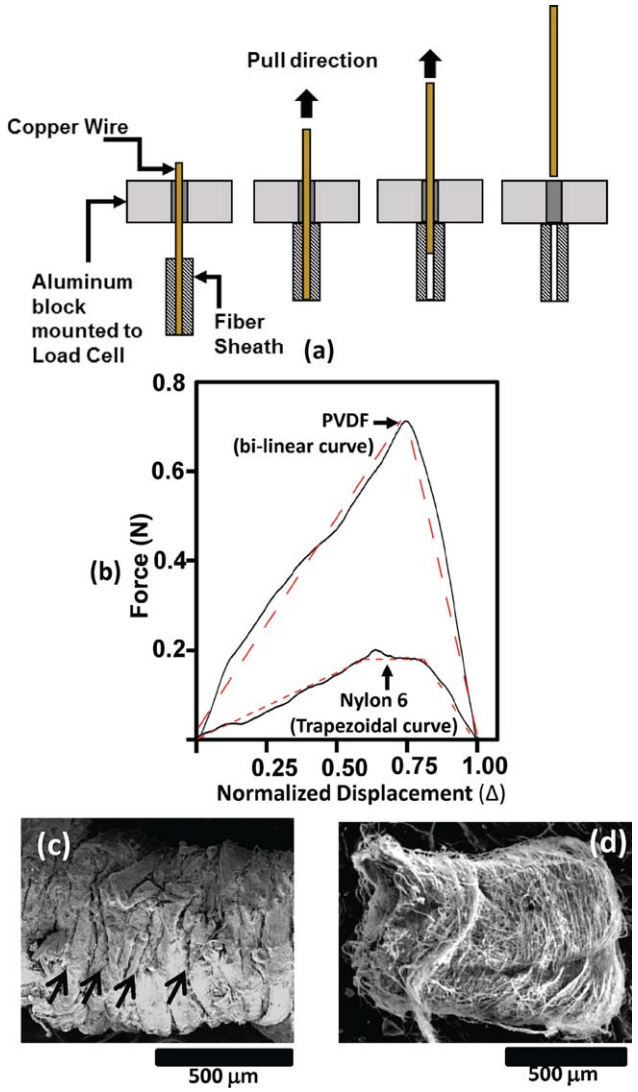

Figure 10. Adhesion strength characterization: (a) testing schematic, (b) load–displacement curve for a 500-μm wire, (c) stripped nylon nanofiber coating, and (d) stripped PVDF nanofiber coating. [Color figure can be viewed in the online issue, which is available at wileyonlinelibrary.com.]

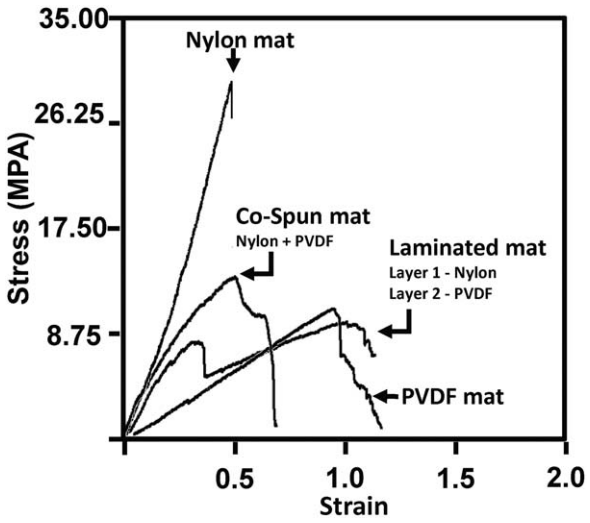

Figure 11. Tensile testing data of the multimaterial nanofiber mats.

Table II. Mechanical Properties of Mats

Material	Young's modulus (MPa)	Ultimate tensile stress (MPa)	Ultimate tensile strain
Nylon mat	87.43 ± 13.43	33.18 ± 9.47	0.48 ± 0.05
PVDF mat	14.62 ± 6.99	8.25 ± 3.18	1.03 ± 0.32
Cospun mat (nylon plus PVDF)	42.52 ± 3.47	13.72 ± 3.55	0.78 ± 0.30
Laminated mat (layer 1 nylon, layer 2 PVDF)	39.66 ± 8.35	9.98 ± 1.27	1.00 ± 0.26

Figure 7(b,c)] were also tested for their tensile properties. The engineering stress–strain curves obtained from these tests are shown in Figure 11, whereas Table II summarizes the material properties obtained from these tests.

Similar to the tensile properties of the nanofiber ropes, the nylon mats were observed to have a high Young's modulus and a high breaking strength when compared to the PVDF mats, which had a high strain-to-failure. The cospun mat was observed to have a blended behavior with a Young's modulus and strain-to-failure value that was between those of the two plain polymer mats. This was in stark contrast to the laminated mat, which showed a sequential failure similar to that of the single-sheath cable. At first, the nylon ply was seen to fail at a strain of 0.35; after this, the PVDF mat took over the load all the way to failure.

CONCLUSIONS

A single scalable manufacturing process was demonstrated for the continuous production of nanofiber-based ropes, cables, microscale wire coatings, and multimaterial mats. The nanofiber ropes, cables, and wire coatings were made with a cascading electrospinning setup in conjunction with a rotating ring collector and a take-up reel. The large-area coating of multimaterial fibrous mats was realized by replacing the ring collector with a directed nozzle. The cascading design of electrospinning units enabled the manufacturing of nanofiber cables with multiple sheaths and material combinations. The tensile failure patterns revealed distinct effects of multimaterial sheaths. The adhesion strength and load–displacement profiles for the nanofiber coating interfaces were observed to be polymer dependent. The large-area nozzle attachment was proven for the generation of coatings and mats. A blended mechanical behavior was observed for cospun fiber mats, whereas a sequential ply failure mode was observed for laminated mats.

ACKNOWLEDGMENTS

The authors acknowledge funding support from the Manufacturing Machines and Equipment Program of the US National Science Foundation (award CMMI 14-62648) and internal funds from Rensselaer Polytechnic Institute.

REFERENCES

1. Lee, S.; Ahn, Y.; Prabu, A.; Kim, K. J. *Fiber Bioeng. Inform.* **2013**, *6*, 369.
2. Agarwal, S.; Wendorff, J. H.; Greiner, A. *Polymer* **2013**, *49*, 5603.
3. Miao, J.; Miyauchi, M.; Simmons, T. J.; Dordick, J. S.; Linhardt, R. J. *J. Nanosci. Nanotechnol.* **2010**, *10*, 5507.
4. Spackman, C.; Picha, K.; Gross, G.; Nowak, J.; Smith, P. J.; Zheng, J.; Samuel, J.; Mishra, S. *ASME J. Micro Nano Manuf.* **2015**, *3*, 011008.
5. Baniasadi, M.; Huang, J.; Xu, Z.; Moreno, S.; Yang, X.; Chang, J.; Quevedo-Lopez, M. A.; Naraghi, M.; Minary-Jolandan, M. *Appl. Mater. Interfaces* **2006**, *7*, 5358.
6. Zander, N. E. *Polymers* **2013**, *5*, 19.
7. Ramakrishna, S.; Fujihara, K.; Teoa, W.; Yong, T.; Ma, Z.; Ramaseshan, R. *Mater. Today* **2006**, *9*, 40.
8. Pan, H.; Li, L.; Cui, X. *Polymer* **2006**, *47*, 4901.
9. He, J.; Zhou, Y.; Wu, Y.; Liu, R. *Surf. Coat. Technol.* **2014**, *258*, 398.
10. Ali, U.; Zhou, Y.; Wang, X.; Lin, T. In Nanofibers—Production, Properties and Functional Applications; Lin, T., Ed.; InTech: Rijeka, Croatia, **2011**; p 153.
11. He, J.; Zhou, Y.; Wang, L.; Liu, R.; Qi, K.; Cui, S. *Fibers Polym.* **2014**, *15*, 2016.
12. Su, C.; Lai, T.; Lu, C.; Liu, Y.; Wu, S. *Fibers Polym.* **2013**, *14*, 542.
13. Cozza, E. S.; Monticelli, O.; Marsano, E.; Cebe, P. *Polym. Int.* **2012**, *62*, 41.
14. Ali, U.; Zhou, Y.; Wang, X.; Lin, T. *J. Text. Inst.* **2012**, *103*, 80.
15. Panthi, G.; Barakat, N. A. M.; Risal, P.; Yousef, A.; Pant, B.; Unnithan, A. R.; Kim, H. Y. *Fibers Polym.* **2013**, *14*, 718.
16. Dabirian, F.; Abdolkarim, S.; Ravandi, H.; Hinestroza, J. P.; Abuzade, R. A. *Polym. Eng. Sci.* **2012**, *52*, 1724.